XPS investigation of titanium contact formation to ZnO nanowires

Chris J. Barnett*[1], Ambroise Castaing, Daniel R. Jones[2], Aled R. Lewis[2], Lewys J. Jenkins[2]
Richard J. Cobley[2] and Thierry G. G. Maffeis[2]

1 Department of Physics, College of Science, Swansea University, Singleton Park, Swansea SA2 8PP, U.K.

2 College of Engineering, Swansea University, Bay Campus, Swansea SA1 8EN, U.K.

c.j.barnett@swansea.ac.uk, a.castaing@swansea.ac.uk, d.r.jones@swansea.ac.uk, 557952@swansea.ac.uk, 520416@swansea.ac.uk, richard.j.cobley@swansea.ac.uk, t.g.g.maffeis@swansea.ac.uk,.

Keywords: ZnO, nanowires, contact, titanium, XPS, Ohmic, Schottky, photoluminescence

Abstract

Ti is often used to form an initial Ohmic interface between ZnO and Au due to its low work function, and the TiO_2/ZnO heterojunction is also of great importance for many practical applications of nanoparticles. Here, Ti has been controllably deposited onto hydrothermally grown ZnO nanowires and the formation of metal-semiconductor contact has been investigated using x-ray photoelectron spectroscopy (XPS), photoluminescence (PL) spectroscopy and scanning electron microscopy (SEM). XPS results showed that that the Ti initially reacts with surface oxygen species to form TiO_2, and further deposition results in the formation of oxides with oxidation state numbers lower than four, and eventually metallic Ti on top of the TiO_2. The formation of TiC was also observed. XPS showed that the onset of metallic Ti coincided with a Zn 3p core level shift to lower binding energy, indicating upwards band bending and the formation of a rectifying contact. . Annealing caused a near-complete conversion of the metallic Ti to TiO_2 and caused the Zn 3p to shift back to its original higher binding energy, resulting in downwards band bending and a more Ohmic contact. PL measurements showed that the optical properties of the nanowires are not affected by the contact formation.

Introduction

ZnO is a metal oxide semiconductor with a wide direct band gap of 3.37eV and a large exciton binding energy of 60 meV that has received much attention over the past 15 years [1, 2]. ZnO can form numerous nanostructures, including nanowires, that have many potential applications in microelectronics [3], mechanical energy harvesting [4], sensors [5], field emitters [6], ultra violet lasers [7], photovoltaics [8] and other optoelectronic devices [9]. All

these devices require the formation of metal/ZnO contacts, the nature of which has profound influence on device performance, with Ohmic contacts preferred for most applications [10, 11]. For nanowire array style devices, where the nanowires grow quasi-vertically from a substrate, one electrical contact can often be made using the seed layer from which the nanowires are grown [5, 12]. To form a similar contact to the free ends of the nanowires, one requires metal deposition using techniques such a sputtering or evaporation [13, 14]. Au is commonly used in contact fabrication as it does not oxidise in air; however, a Schottky contact forms when it is deposited on ZnO [15]. Therefore Ti is often used to form an initial Ohmic interface between the ZnO and Au due to its low work function [10, 16, 17]. A drawback of this approach is that Ti is extremely reactive and oxygen atoms out-diffuse from the ZnO into the Ti layer to form TiO_2 [18], which can cause a high contact resistance. Conversely, the formation of oxygen vacancies near the ZnO surface can increase carrier concentration and lower specific contact resistance [19]. The TiO_2/ZnO heterojunction is also of great importance for dye sensitised solar cells,[20, 21], photocatalysis[22-24], water-splitting and self-cleaning coatings [25]. It is therefore important to understand the formation of the Ti/ZnO contacts and the TiO_2/ZnO heterojunction in order to optimise device performances.

Here, we controllably deposit Ti onto hydrothermally grown ZnO nanowires and investigate the formation of the metal-semiconductor contact using x-ray photoelectron spectroscopy (XPS), photoluminescence (PL) and scanning electron microscopy (SEM).

Experimental Methods

ZnO nanowires were synthesised hydrothermally on a Si substrate with a 30 nm ZnO seed layer using a 1:1 molar ratio solution of zinc nitrate and hexamethylenetetramine held at 90^{o}C for 9 hours [26]. We tested two samples made using this procedure and it was found during the initial XPS analysis that one of the samples (hereafter referred to Sample 2) had more surface oxygen species than the other (to be referred to as Sample 1). This discrepancy is likely due to storage time between synthesis and experiment and will be discussed further later in the paper. The nanowires were characterised with SEM (Hitachi S4800) and PL (Melles-Griot 325 nm He-Cd laser and Ocean Optics USB2000+ spectrometer) prior to loading into the XPS chamber (Thermo Scientific Escalab Mk 3, base pressure 10^{-10} mbar). The sample was scanned with XPS before and after each Ti deposition step. The Ti was deposited onto the nanowires using an *in-situ* e-beam evaporation source (Oxford Instruments EGN4) for increasing amounts of time. The thickness was determined from the deposition time by prior calibration of the source using a quartz crystal microbalance. The thickness of each deposition step is shown in Table 1. After the final deposition the sample was removed from vacuum, re-characterised with PL and SEM then annealed in a nitrogen atmosphere at 300^{o}C for 3 minutes and allowed to cool naturally [27]. This annealing step is typical for the fabrication of Ohmic contacts between n-type ZnO and Ti [28-30]. Following the final annealing step, the sample was characterised once more by SEM and PL and then reloaded into the XPS and scanned a final time.

Thickness deposited (nm)	0.2	0.2	0.4	0.8	1.6	3.2	6.4
Total thickness (nm)	0.2	0.4	0.8	1.6	3.2	6.4	12.8

Table 1: sequence of Ti deposition steps and total thickness deposited.

Results and Discussion

Figure 1 shows top down SEM images of the nanowires before and after 12.8 nm Ti deposition and after annealing. The as-grown nanowires exhibited the typical ZnO hexagonal cross-section, with an average diameter of 48.1 ± 1.2 nm and an average length of 1.70 ± 0.10 μm. After Ti deposition the nanowire surface became rougher, with the hexagonal facets no longer distinguishable and the mean diameter increasing to 63.3± 1.5 nm. Annealing resulted in an apparent "smoothing" of the surface with the hexagonal facets becoming visible under SEM and a reduction in diameter to 50.7± 1.4 nm, suggesting the titanium had diffused into the ZnO nanowires. Ti evaporation can be ruled out because of the very low vapour pressure of Ti at 300^{o}C and the Ti 2p core level intensity, discussed later in the text.

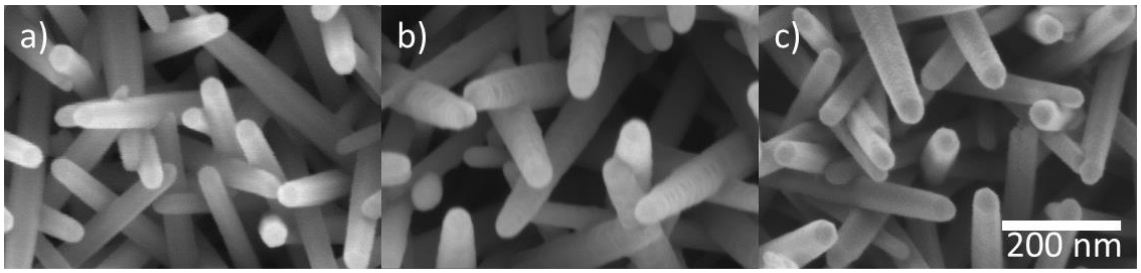

Figure 1: SEM images of ZnO nanowires a) before Ti deposition, b) after Ti deposition (12.8 nm) and c) after annealing (Sample 2).

XPS scans were recorded following each stage of the Ti deposition procedure, including a survey spectrum and detailed spectra of the Zn 2p, Zn 3p, O 1s, C 1s, and Ti 2p core levels. Figure 2 depicts the changes of the survey scans and Ti 2p core level for Sample 2 with increasing Ti coverage and following the anneal. The same features and trends were observed for Sample 1. After the first Ti deposition of 0.2 nm, the spectrum consists of a peak centred at 458.5 eV which is attributed to the Ti $2p_{3/2}$ level for TiO_2 (Ti^{4+}) [31], suggesting that the

titanium reacted with the surface oxygen of the nanowires, possibly sourced from OH^- groups.

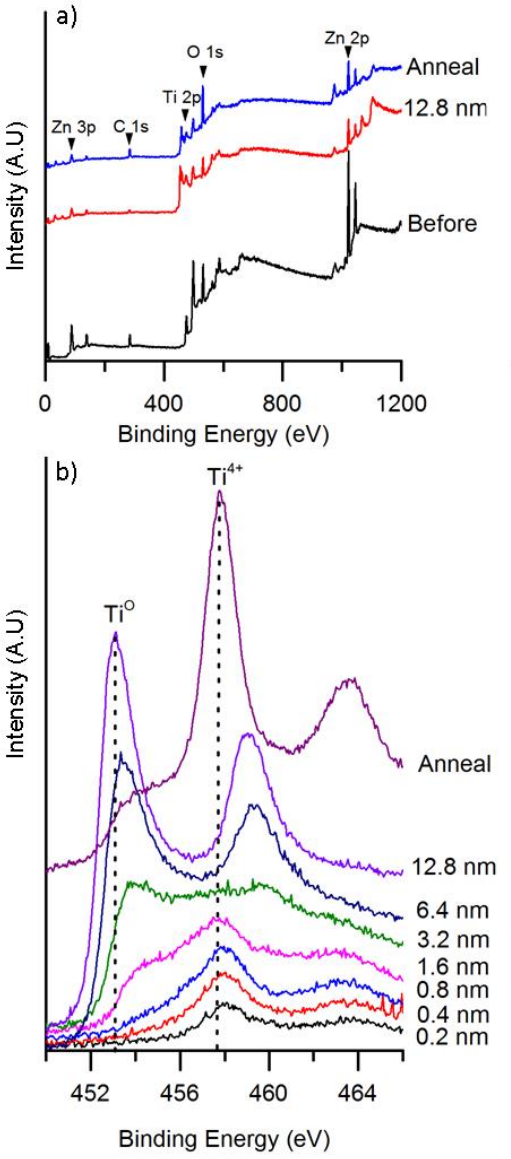

Figure 2: a) Evolution of the survey scans before Ti deposition, after 12.8 nm of Ti deposition and after the final annealing step. b) Evolution of the Ti 2p core level in Sample 2 with increasing Ti thickness and after the final annealing step. The spectrum from the annealed step is offset vertically for clarity.

As the thickness of Ti increased, more features appeared on the lower binding energy side of the TiO_2 peak. These features are attributed to lower oxidation states of Ti (Ti^{3+}, Ti^{2+}, Ti^{+}) and TiC, as well as TiCO [32]. The lowest energy feature, centred 4.8 eV lower then TiO_2 peak and clearly visible at 6.4 and 12.8 nm coverage, is likely to correspond to metallic Ti [31]. The corresponding metallic Ti $2p_{1/2}$ peak is also visible at 6 eV higher binding energy, in agreement with data within the literature [31]. These features indicate that the majority of deposited titanium was no longer reacting with surface oxygen at this stage of the deposition, and thus remains in a metallic state. Exposing the sample to air and annealing in nitrogen at 300^{o}C caused the peaks corresponding to metallic Ti to decrease and the TiO_2 peak to dominate.

Figure 3 shows the progression of the O 1s peaks of Sample 1 and Sample 2 during Ti deposition. Prior to Ti deposition, the O 1s peak of both samples consisted of a main component centred at 530.2 eV, which may be attributed to lattice oxygen, and a shoulder on the higher binding energy side caused by surface oxygen and commonly attributed to hydroxide ions [33-35]. Previous works have fitted this surface contribution with one or two components [33-35] and in this work, consistent with our previous publication [36], we fitted the surface contribution to the O 1s core level with two components: the component located 1.35 eV from the main lattice oxygen component and denoted S1 is attributed to hydroxide ions, while the second component, which is centred 2.3e V from the lattice oxygen component and shall be referred to as S2, is thought to correspond to water vapour. It should be noted that this interpretation is speculative as our previous result [36] suggested that the middle component could comprise of two different bonds with similar binding energy. Additionally, the surface components have also been attributed to oxygen bonded to carbon or oxygen vacancies and other sub-surface defects [37-39].

It is clear from Figure 3 that the contribution of the surface oxygen is significantly larger (99% of the lattice oxygen component, calculated using the areas of the oxygen lattice component and the surface oxygen components) for Sample 2 than in the case of Sample 1 (52% of the lattice component), indicating higher quantities of surface oxygen. The difference is probably due to the fact that Sample 2 was stored for 12 months prior to the experiment, whilst Sample 1 was scanned almost immediately after growth. Different humidity conditions during synthesis could also be a factor. Figure 3 shows that, for both samples, the surface oxygen components decreased in intensity relative to the main lattice oxygen component with Ti deposition up to 1.6 nm coverage (see inset), as the Ti reacts with the surface oxygen to form TiO_2 and TiO_x ($x<2$) species. From the 3.2 nm deposition step onward, the surface oxygen component intensity does not decrease anymore, indicating that the surface oxygen has stopped reacting with the Ti. This also corresponds to the point where TiC and metallic Ti begin to appear on the Ti 2p core level (Figure 2).

The O 1s peak also broadened after the 6.4 nm and 12.8 nm Ti deposition steps, which is indicative of the formation of new species with a higher binding energy than the lattice oxygen of ZnO. These components may be attributed to TiO_x ($x<2$) species as well as TiCO, suggesting that some of the deposited Ti may have begun to react with the lattice oxygen. The position of the O 1s peak shifted by 0.6 eV to lower binding energy after annealing, which likely corresponds to a chemical shift resulting from the oxidation of the metallic Ti to TiO_2. The broad shoulder on the high binding energy side is probably caused by the underlying ZnO and also surface oxygen species. This interpretation is supported by previous work such as Rtimi *et al*. [40], who reported that the O 1s core level binding energy for TiO is 1.4 eV greater than for TiO_2, and Kumar *et al*. [41], who identified a 1.8 eV gap between

the two chemical states. The TiO_2 that formed initially following the first few Ti depositions, which was clearly apparent in the Ti 2p spectra is not readily observed within the O 1s spectra, probably because it provides a much smaller contribution than the oxygen contained within the ZnO lattice.

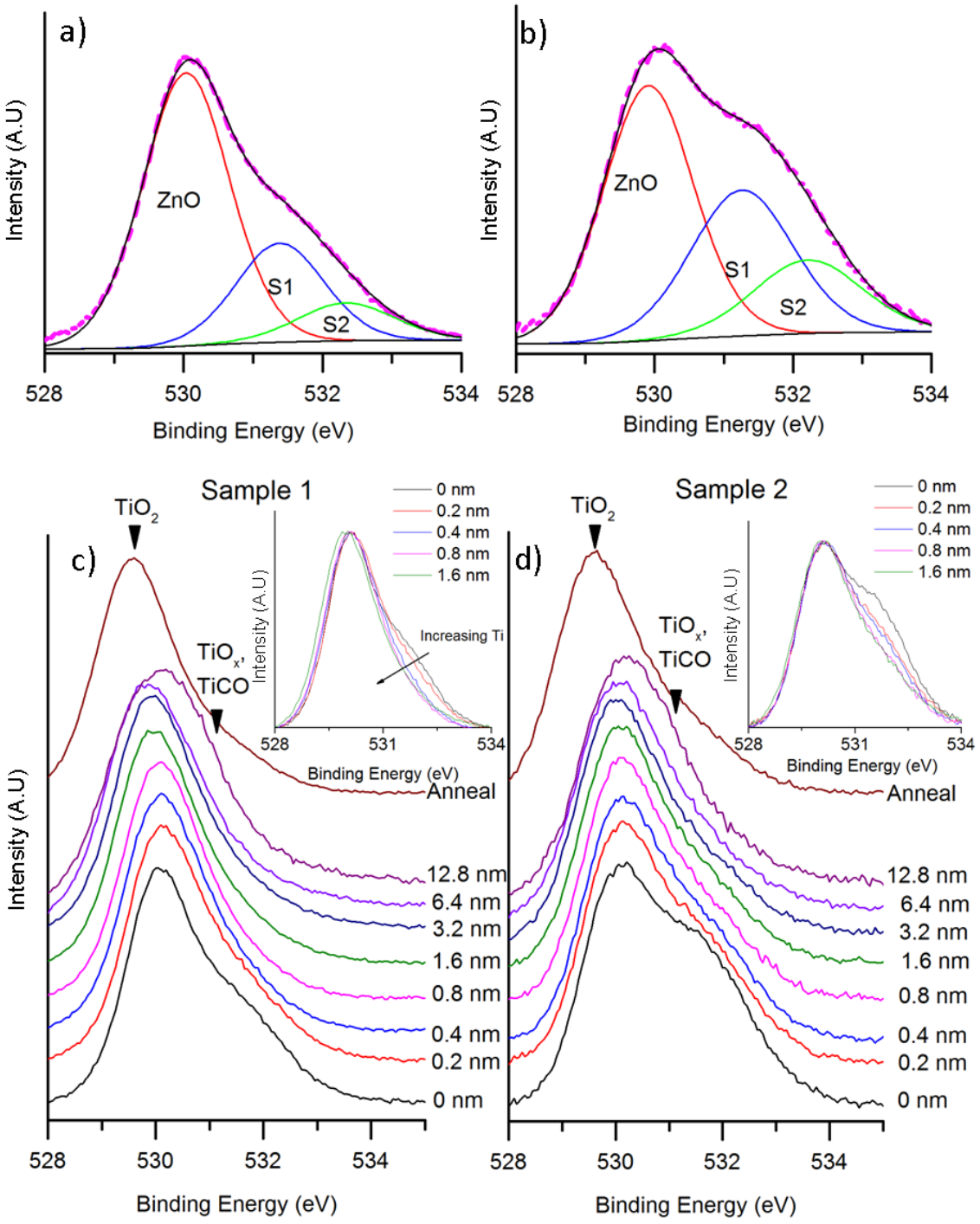

Figure 3: The O 1s peak before Ti deposition, showing fits and background for a) Sample 1 and b) Sample 2. Evolution of the O 1s with increasing Ti thickness and following the final annealing step for c) Sample 1 and d) Sample 2. Insets show overlay

of the O 1s core level peak-shape with increasing Ti thickness up to 1.6 nm, showing the reduction in the surface oxygen components.

The evolution of the C 1s core level is plotted in Figure 4 for Sample 1. Initially the C 1s peak consisted of a main component centred at 284.4 eV, which may be attributed to C-C and C-H bonding resulting from ambient hydrocarbon contamination. After 3.2 nm Ti deposition, a second component centred at a binding energy 3 eV lower than the main component appeared, which likely corresponds to the formation of TiC [42, 43]. These results, together with the O1s results, suggest that the deposited Ti initially reacted with surface oxygen up to 1.6 nm thickness, whereas the formation of TiC occurred at Ti coverages greater than 1.6 nm. This suggests that Ti reacted preferentially with surface oxygen and only started to form TiC once the available surface oxygen had been consumed in the formation of TiO_2. This is in agreement with the evolution of the O1s core level peak shape of Figure 3 which shows that the decrease in surface oxygen stopped at Ti coverage greater than 1.6 nm. Following the anneal, the hydrocarbon contribution increased greatly due to exposure to ambient air but the TiC component remained, although with diminished intensity due to the enhanced surface contamination.

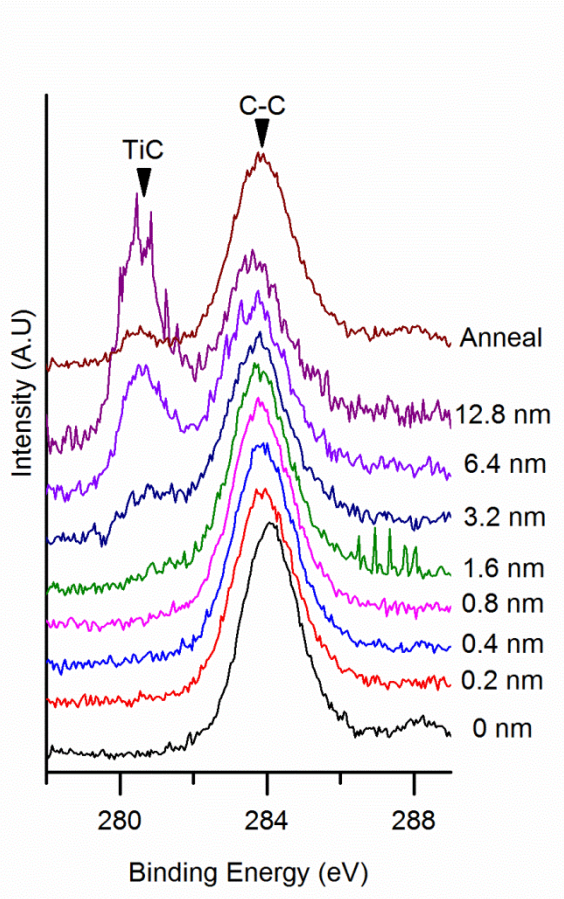

Figure 4: Evolution of the C 1s core level with increasing Ti thickness and following the final annealing step. The spectra are offset vertically for clarity.

Figure 5 shows Zn 3p normalised spectra for both samples. It is known that the Zn 3p core level binding energy (as well as the Zn 2p) is almost independent of the type of chemical bonds [44] and, as expected, we did not observe any significant change in the Zn 3p or 2p peak envelope with Ti deposition. The Zn core levels are therefore good indicators of band bending for semiconductors as they are affected negligibly by chemical shifts [45]. Figure 5 show that up to 1.6 nm Ti thickness, no Fermi shift was observed. This indicates that there was no electron transfer between the ZnO and TiO_2, as might be expected from the small difference in electron affinity between the two semiconductors [46]. A small, gradual shift to lower binding energy between the 1.6 nm and 12.8 nm thicknesses was observed for both

sample. The total shift was 0.4 eV for Sample 1, whilst a smaller shift of 0.15 eV was observed in the case of Sample 2. These shifts were also apparent on the O 1s core level until the 12.4 nm deposition, where the contribution of TiO_x species distorted the peak envelope. The shifts indicate upwards band bending resulting in a more rectifying contact.

Annealing caused the Zn 3p peak of both samples to shift back to the binding energy measured for the pre-deposition surface. It is therefore evident that the annealing step counteracted the potential barrier at the interface between Ti and ZnO, thereby resulting in a more ohmic contact, despite the procedure leading to extensive oxidation of the Ti. The fact that Sample 2 exhibited a smaller shift in binding energy compared to Sample 1 is likely to be due to sample 2 possessing higher amounts of oxygen present at its surface. The oxygen species may act as either donors or acceptors depending on their exact nature: hydroxyl groups, for example, behave as donors [33], whilst oxygen ions are acceptors [47]. Both species therefore influence surface band bending and create surface states which may pin the Fermi level [48]. For this reason, it is likely that Sample 2 exhibited a higher density of surface states than Sample 1 prior to Ti deposition. As the Ti was deposited, it consumed some of the ZnO surface oxygen species to form TiO_2 but a significant amount remained: from zero to 1.6 nm coverage, the surface oxygen to lattice oxygen ratio for Sample 1 and Sample 2 decreased from 52% to 26% and from 99% to 42%, respectively.

The fact that not all the surface oxygen was consumed by the Ti hints at the presence of two types of surface oxygen, in good agreement with our previous work [47]. In this earlier paper, we studied the effect of UHV annealing on ZnO nanowires and found that whilst annealing at 300°C in UHV removed around half of the surface oxygen, additional annealing steps up to 600°C resulted in no further measurable change. For Ti thicknesses greater than 1.6 nm, the

amount of surface oxygen stopped decreasing and less oxidised Ti species began to form, as the deposited Ti stopped reacting with surface oxygen. Metallic Ti then became apparent at thicknesses above 3.2 nm. It is probable that transfer of electrons occurred from the ZnO to the metallic Ti, leading to upward band bending and the associated formation of a slightly rectifying contact. However, due to the likelihood that a higher concentration of surface states existed in Sample 2 than Sample, it is possible that the band bending resulting from the presence of metallic Ti was less pronounced in the case of Sample 2 as the Fermi level may have been partially pinned by the surface states. For both samples, however, the N_2 anneal negated the effect of the Ti by converting most of the metallic Ti to TiO_2.

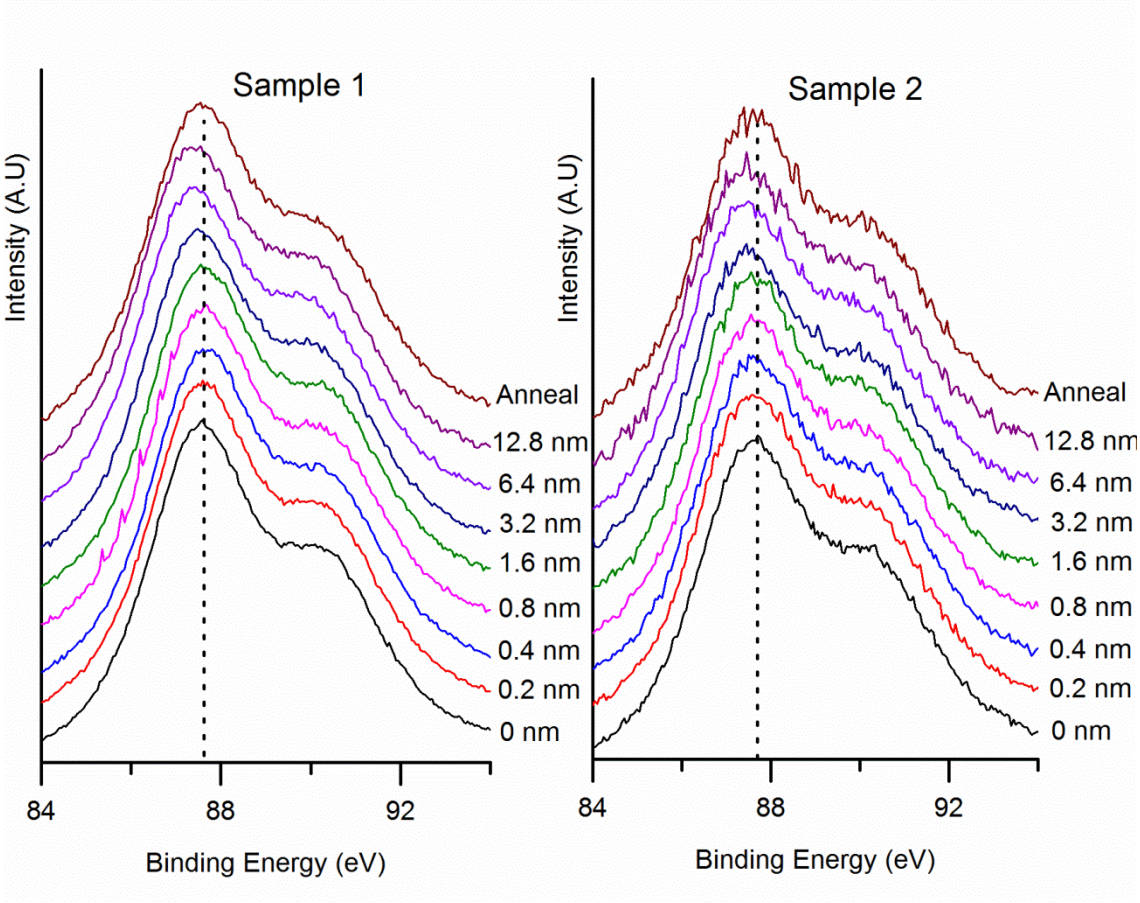

Figure 5: Evolution of the Zn 3p core level with increasing Ti thickness and following the final annealing step for sample 1 and 2. The spectra are offset vertically for clarity. The dotted line is a guide to the eye emphasising the small binding energy shifts.

Figure 6 shows the evolution of the normalised intensity of the measured core levels as a function of Ti thickness and following the post deposition anneal for Sample 2. The Ti 2p intensity decreased slightly after annealing whilst the intensity of both Zn core levels remained the same. These trends may be attributed to the diffusion of Ti into the ZnO nanowires, which also accounts for the decrease in diameter and the "smoothing" of the facets observed in the SEM image of Figure 1c. The O 1s intensity remained almost constant up to 1.6 nm thickness whilst the C 1s and Zn core levels decreased. This behaviour is consistent with the formation of TiO_2 at the surface of the nanowires observed in the Ti 2p spectra. At thicknesses above 1.6 nm, the C 1s intensity decreased less sharply than during the initial depositions, and this can be correlated to the onset of TiC formation at the surface, as evident from the C 1s spectra.

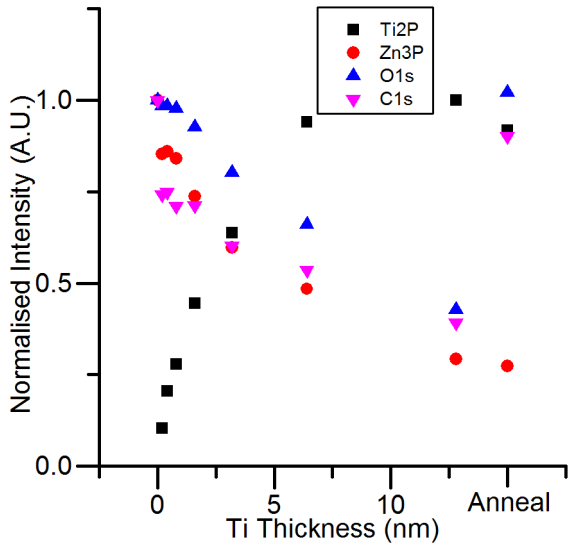

Figure 6. Normalised peak intensity of the O 1s, C 1s, Zn 3p and Ti 2p against Ti thickness and following the final annealing step. The intensities are normalised to their initial values (before Ti deposition)

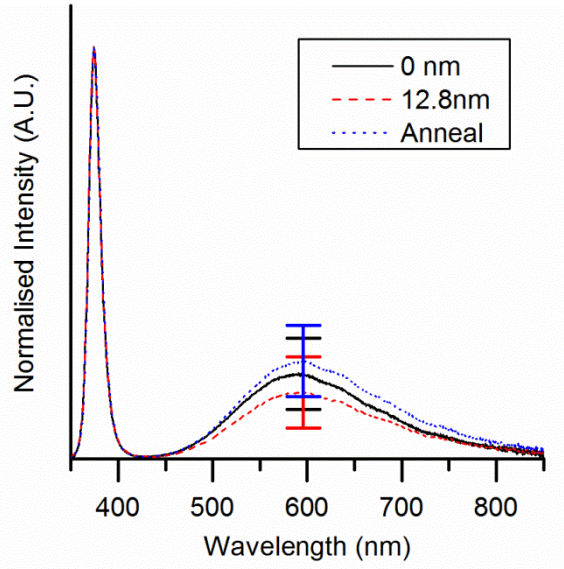

Figure 7. Normalised PL spectra of ZnO nanowires before Ti deposition, after 12.8 nm of Ti deposition and after the final anneal. Error bars indicate the standard deviation across the sample.

In order to investigate the effects of the contact formation on the optical properties of the nanowires, PL spectra were recorded before Ti deposition, after Ti deposition and after the anneal. The PL spectra are shown in Figure 7 and are normalised to the near band edge (NBE) peak intensity, which always remained centred at a wavelength of 374.7 nm, to allow direct comparison between the three cases. The position and shape of the deep level emission peak also stayed constant, and the location of the peak maximum at a wavelength of 595 nm indicates that oxygen vacancies were the main contributors to the emission [18, 49]. Ti deposition and annealing in nitrogen at 300^{o}C did not significantly alter the deep level band. This suggests that the deep level band was not affected by modification of the surface, unlike previously published results where surfactants were highly efficient in suppressing deep level emission [50]. Similarly, annealing in Ar at 700^{o}C has been reported to completely suppress

the deep level emission [51]. Our results, however, show that the 300°C anneal in nitrogen had no effect on the optical properties of the nanowires. The optical properties were therefore preserved after contact formation, a result which could be beneficial for optoelectronic devices. Additionally, the PL results indicate that the Ti diffused into the lattice during the anneal, rather than lattice oxygen diffusing out[u1] and creating oxygen vacancies which would have altered the deep level emission. It is likely that the conversion of the metallic Ti to TiO_2 occurred as soon as the sample was removed from vacuum and exposed to air, rather than reaction with lattice oxygen during the anneal. This is in agreement with the SEM images and the XPS intensity data.

Conclusions

Following hydrothermal synthesis of ZnO nanowires, the stepped formation of a titanium contact and the effect of subsequently annealing in nitrogen at 300°C have been studied using XPS, SEM and PL. For thicknesses up to 0.8 nm, the Ti reacted with surface oxygen species to form TiO_2. Increased Ti deposition (from 1.6 nm thickness) resulted in the formation of Ti oxides with a lower oxidation state number, and eventually metallic Ti. It was also observed that the Ti reacted with surface carbon contamination forming TiC and possibly TiCO for Ti thicknesses of 3.2 nm or higher. Exposure to air and annealing the sample resulted in a conversion to TiO_2, with little metallic Ti or TiC present at the surface.

The appearance of metallic Ti, following Ti deposition of thickness greater than 3.2 nm, caused the binding energy of the Zn 3p signal to shift to lower values, indicating upwards band bending and the formation of a rectifying contact. [u2]Moreover, annealing resulted in the diffusion of Ti into the ZnO nanostructure, yielding a surface consisting mostly of TiO_2. The formation of the Ti contact was investigated on two different samples, which produced

very similar behaviour, confirming the reproducibility of the results. The only discernible difference between the two samples concerned the magnitude of the band bending caused by the metallic Ti, which was attributed to the different amount of initial surface oxygen present on the two samples. Finally, PL results showed that the formation of the contact did not alter the optical properties of the nanowires, which is beneficial for the realisation of optoelectronics devices.

These results provide insights into the complex ZnO/Ti interface formation and have implications for ZnO nanowire device manufacture where Ti is intended as an ohmic contact and also for devices that make use of ZnO/TiO_2 heterojunctions.

Competing interests

The authors declare that they have no competing interests.

Acknowledgements

This work was part funded through an EPSRC doctoral training award and a Royal Society university Research Fellowship.

References

[1] Tarat A, Majithia R, Brown R, Penny M and Meissner K 2012 Synthesis of nanocrystalline ZnO nanobelts via pyrolytic decomposition of zinc acetate nanobelts and their gas sensing behavior *Surf Sci* **606** 715 - 21

[2] Schmidt-Mende L and MacManus-Driscoll J L 2007 ZnO - nanostructures, defects, and devices *Materials Today* **10** 40-8
[3] Chang P-C, Fan Z, Chien C-J, Stichtenoth D, Ronning C and Lu J G 2006 High-performance ZnO nanowire field effect transistors *APPLIED PHYSICS LETTERS* **89** 133113
[4] Qin Y, Wang X and Wang Z L 2008 Microfibre-nanowire hybrid structure for energy scavenging *Nature* **451** 809-13
[5] Lloyd J S, Fung C M, Deganello D, Wang R J, Maffeis T G G, Lau S P and Teng K S 2013 Flexographic printing-assisted fabrication of ZnO nanowire devices *Nanotechnology* **24** 195602
[6] Zhu Y, Zhang H, Sun X, Feng S, Xu J, Zhao Q, Xiang B, Wang R and Yu D 2003 Efficient field emission from ZnO nanoneedle arrays *APPLIED PHYSICS LETTERS* **83** 144-6
[7] Huang M H, Mao S, Feick H, Yan H Q, Wu Y Y, Kind H, Weber E, Russo R and Yang P D 2001 Room-temperature ultraviolet nanowire nanolasers *Science* **292** 1897-9
[8] Luo Q, Wu Z, He J, Cao Y, Bhutto W, Wang W, Zheng X, Li S, Lin S, Kong L and Kang J 2015 Facile synthesis of composition-tuned ZnO/ZnxCd1-xSe nanowires for photovoltaic applications *Nanoscale Research Letters* **10** 181
[9] Willander M 2014 Nano-lasers and nano-LEDs *Journal of Physics: Conference Series* **486** 012030
[10] Lee J-M, Kim K-K, Park S-J and Choi W-K 2001 Low-resistance and nonalloyed ohmic contacts to plasma treated ZnO *APPLIED PHYSICS LETTERS* **78** 3842-4
[11] Sheng H, Emanetoglu N W, Muthukumar S, Feng S and Lu Y 2002 Nonalloyed Al ohmic contacts to MgxZn1−xO *Journal of Electronic Materials* **31** 811-4
[12] Smith N A, Evans J E, Jones D R, Lord A M and Wilks S P 2015 Growth of ZnO nanowire arrays directly onto Si via substrate topographical adjustments using both wet chemical and dry etching methods *Materials Science and Engineering: B* **193** 41-8
[13] Wu W, Wen X and Wang Z L 2013 Taxel-Addressable Matrix of Vertical-Nanowire Piezotronic Transistors for Active and Adaptive Tactile Imaging *Science* **340** 952-7
[14] Latu-Romain E, Gilet P, Noel P, Garcia J, Ferret P, Rosina M, Feuillet G, Lévy F and Chelnokov A 2008 A generic approach for vertical integration of nanowires *Nanotechnology* **19** 345304
[15] Kim S-H, Kim H-K and Seong T-Y 2005 Electrical characteristics of Pt Schottky contacts on sulfide-treated n-type ZnO *APPLIED PHYSICS LETTERS* **86** 022101
[16] Murphy T E, Blaszczak J O, Moazzami K, Bowen W E and Phillips J D 2005 Properties of electrical contacts on bulk and epitaxial n-type ZnO *Journal of Electronic Materials* **34** 389-94
[17] Oh M-S, Kim S-H, Hwang D-K, Park S-J and Seong T-Y 2005 Formation of Low Resistance Nonalloyed Ti／Au Ohmic Contacts to n-Type ZnO by KrF Excimer Laser Irradiation *Electrochemical and Solid-State Letters* **8** G317-G9
[18] Kim H-K, Kim S-W, Yang B, Kim S-H, Lee K H, Ji S H and Yoon Y S 2006 Electrical and Interfacial Properties of Nonalloyed Ti/Au Ohmic and Pt Schottky Contacts on Zn-Terminated ZnO *Japanese Journal of Applied Physics* **45** 1560
[19] Chen J-J, Jang S, Anderson T J, Ren F, Li Y, Kim H-S, Gila B P, Norton D P and Pearton S J 2006 Low specific contact resistance Ti*/*Au contacts on ZnO *APPLIED PHYSICS LETTERS* **88** 122107
[20] Wu K, Yu Y, Shen K, Xia C and Wang D 2013 Effect of ultra-thin ZnO coating layer on the device performance of TiO2 dye sensitized solar cell *Solar Energy* **94** 195-201
[21] Ulusoy T G, Ghobadi A and Okyay A K 2014 Surface engineered angstrom thick ZnO-sheathed TiO2 nanowires as photoanodes for performance enhanced dye-sensitized solar cells *Journal of Materials Chemistry A* **2** 16867-76
[22] Chen J, Liao W, Jiang Y, Yu D, Zou M, Zhu H, Zhang M and Du M 2016 Facile Fabrication of ZnO/TiO2 Heterogeneous Nanofibres and Their Photocatalytic Behaviour and Mechanism towards Rhodamine B
[23] Xiao F-X 2012 Construction of highly ordered ZnO–TiO2 nanotube arrays (ZnO/TNTs) heterostructure for photocatalytic application *ACS Applied Materials & Interfaces* **4** 7055-63

[24] Chen Y, Zhang C, Huang W, Yang C, Huang T, Situ Y and Huang H 2014 Synthesis of porous ZnO/TiO 2 thin films with superhydrophilicity and photocatalytic activity via a template-free sol–gel method *Surface and Coatings Technology* **258** 531-8
[25] Wang R, Tan H, Zhao Z, Zhang G, Song L, Dong W and Sun Z 2014 Stable ZnO@TiO2 core/shell nanorod arrays with exposed high energy facets for self-cleaning coatings with anti-reflective properties *Journal of Materials Chemistry A* **2** 7313-8
[26] Barnett C J, Brown R A, Jones D R, Tarat A, Cobley R J and Maffeis T G G 2012 Investigation into the initial growth parameters of hydrothermally grown zinc oxide nanowires*20-23 Aug. 2012)* p 1-4
[27] Tiong T Y, Yahaya M, Dee C F, Salleh M M and Majlis B Y 2008 Study of the contact properties of ZnO nanowires with Ag and Au/Ag*25-27 Nov. 2008)* p 558-60
[28] Fijol J F and Holloway P H 1996 Ohmic Contacts to ZnSe-Based Materials *Critical Reviews in Solid State and Materials Sciences* **21** 77-128
[29] Young Kim S, Won Jang H, Kyu Kim J, Min Jeon C, Il Park W, Yi G-C and Lee J-L 2002 Low-resistance Ti/Al ohmic contact on undoped ZnO *Journal of Electronic Materials* **31** 868-71
[30] Kim H-K, Han S-H, Seong T-Y and Choi W-K 2001 Electrical and Structural Properties of Ti/Au Ohmic Contacts to n - ZnO *Journal of The Electrochemical Society* **148** G114-G7
[31] Biesinger M C, Lau L W M, Gerson A R and Smart R S C 2010 Resolving surface chemical states in XPS analysis of first row transition metals, oxides and hydroxides: Sc, Ti, V, Cu and Zn *Applied Surface Science* **257** 887-98
[32] Ottakam Thotiyl M M, Freunberger S A, Peng Z, Chen Y, Liu Z and Bruce P G 2013 A stable cathode for the aprotic Li–O2 battery *Nat Mater* **12** 1050-6
[33] Heinhold R, Cooil S P, Evans D A and Allen M W 2014 Stability of the Surface Electron Accumulation Layers on the Nonpolar ($10\bar{1}0$) and ($11\bar{2}0$) Faces of ZnO *The Journal of Physical Chemistry C* **118** 24575-82
[34] Byrne D, McGlynn E, Henry M O, Kumar K and Hughes G 2010 A novel, substrate independent three-step process for the growth of uniform ZnO nanorod arrays *Thin Solid Films* **518** 4489-92
[35] Crist B V 2005 PDF Handbooks of Monochromatic XPS Spectra Volume 2 *Pure Binary Oxides*
[36] Maffeis T G G, Penny M W, Castaing A, Guy O J and Wilks S P 2012 XPS investigation of vacuum annealed vertically aligned ultralong ZnO nanowires *Surface Science* **606** 99-103
[37] Lupan O, Pauporté T, Tiginyanu I M, Ursaki V V, Şontea V, Ono L K, Cuenya B R and Chow L 2011 Comparative study of hydrothermal treatment and thermal annealing effects on the properties of electrodeposited micro-columnar ZnO thin films *Thin Solid Films* **519** 7738-49
[38] Lupan O, Chow L, Chai G, Roldan B, Naitabdi A, Schulte A and Heinrich H 2007 Nanofabrication and characterization of ZnO nanorod arrays and branched microrods by aqueous solution route and rapid thermal processing *Materials Science and Engineering: B* **145** 57-66
[39] Seokhwan B, Seungjun L, Joohyun P, Soyeon P, Wooho J and Hyeongtag J 2009 Investigation of the effects of interface carrier concentration on ZnO thin film transistors fabricated by atomic layer deposition *Journal of Physics D: Applied Physics* **42** 235102
[40] Rtimi S, Nesic J, Pulgarin C, Sanjines R, Bensimon M and Kiwi J 2014 Effect of surface pretreatment of TiO2 films on interfacial processes leading to bacterial inactivation in the dark and under light irradiation *Interface Focus* **5**
[41] Kumar P M, Badrinarayanan S and Sastry M 2000 Nanocrystalline TiO2 studied by optical, FTIR and X-ray photoelectron spectroscopy: correlation to presence of surface states *Thin Solid Films* **358** 122-30
[42] Cheng Y and Zheng Y F 2007 Characterization of TiN, TiC and TiCN coatings on Ti–50.6 at.% Ni alloy deposited by PIII and deposition technique *Surface and Coatings Technology* **201** 4909-12

[43] Stüber M, Leiste H, Ulrich S, Holleck H and Schild D 2002 Microstructure and properties of low friction TiC・C nanocomposite coatings deposited by magnetron sputtering *Surface and Coatings Technology* **150** 218-26
[44] Gao Y K, Traeger F, Shekhah O, Idriss H and Wöll C 2009 Probing the interaction of the amino acid alanine with the surface of ZnO *Journal of Colloid and Interface Science* **338** 16-21
[45] Dar T A, Agrawal A, Misra P, Kukreja L M, Sen P K and Sen P 2014 Valence and conduction band offset measurements in Ni0.07Zn0.93O/ZnO heterostructure *Current Applied Physics* **14** 171-5
[46] Conesa J C 2012 Modeling with Hybrid Density Functional Theory the Electronic Band Alignment at the Zinc Oxide–Anatase Interface *The Journal of Physical Chemistry C* **116** 18884-90
[47] Lord A M, Maffeis T G, Allen M W, Morgan D, Davies P R, Jones D R, Evans J E, Smith N A and Wilks S P 2014 Surface state modulation through wet chemical treatment as a route to controlling the electrical properties of ZnO nanowire arrays investigated with XPS *Applied Surface Science* **320** 664-9
[48] Malagù C, Carotta M C, Galliera S, Guidi V, Maffeis T G G, Martinelli G, Owen G T and Wilks S P 2004 Evidence of bandbending flattening in 10 nm polycrystalline SnO2 *Sensors and Actuators B: Chemical* **103** 50-4
[49] Ra H-W, Choi K S, Ok C W, Jo S Y, Bai K H and Im Y H 2008 Ion bombardment effects on ZnO nanowires during plasma treatment *APPLIED PHYSICS LETTERS* **93** -
[50] Djurisic A, Choy W, Roy V, Leung Y, Kwong C, Cheah K, Gundu Rao T, Chan W, Fei Lui H and Surya C 2004 Photoluminescence and electron paramagnetic resonance of ZnO tetrapod structures *Adv Funct Mater* **14** 856 - 64
[51] Bekeny C, Voss T, Gutowski J, Postels B, Kreye M and Waag A 2007 Optical properties of ZnO nanorods realised by aqueous chemical growth *Superlattices and Microstructures* **42** 398-402